Hindawi
Journal of Nanomaterials
Volume 2022, Article ID 2110636, 12 pages
https://doi.org/10.1155/2022/2110636

Research Article

Biosynthesis of Silver Nanoparticles from *Rhododendron arboreum* for Metal Sensing, Antibacterial Assessment, and Photocatalytic Degradation

Sitaram Phuyal,[1] **Ganesh Lamichhane**,[1] **Aakash Gupta**,[2] **Karan Khadayat**,[1] **Anup Adhikari**,[1] **Rishab Marahatha**,[1] **Sujan Khadka**,[3] **and Niranjan Parajuli**[1]

[1]*Biological Chemistry Lab, Central Department of Chemistry, Tribhuvan University, Kirtipur, Kathmandu 44600, Nepal*
[2]*Department of Chemistry and Biochemistry, University of Massachusetts Dartmouth, North Dartmouth, Massachusetts 02747, USA*
[3]*Department of Microbiology, Birendra Multiple Campus, Tribhuvan University, Bharatpur, Chitwan 44207, Nepal*

Correspondence should be addressed to Niranjan Parajuli; niranjan.parajuli@cdc.tu.edu.np

Received 7 March 2022; Revised 19 May 2022; Accepted 31 May 2022; Published 14 June 2022

Academic Editor: Lavinia Balan

The nanomaterial industry has focused on green synthetic methods to avoid unpleasant compounds produced during manufacturing, offering eco-friendly, sustainable, and nature-derived alternative methods. In this study, silver nanoparticles (Ag NPs) have been synthesized from an aqueous extract of the leaves of *Rhododendron arboreum*, where the pH of the reaction mixture is found to be crucial. The reaction progress monitored using the UV-Vis spectrophotometer displayed a strong absorption band at 425 nm at pH 9, suggesting an optimum pH for the synthesis. The Ag NPs thus synthesized were characterized using instrumental techniques. The attenuated total reflectance-Fourier transform infrared (ATR-FTIR) spectroscopy showed the presence of phytoconstituents in the aqueous extract, which are believed to be responsible for reducing Ag^+ ions to Ag NPs and capping agents on its surface for stability. X-ray diffraction (XRD) showed a highly crystalline nature, and energy-dispersive X-ray (EDX) demonstrated the presence of metallic silver. The scanning and transmission electron microscopy (SEM and TEM, respectively) revealed crystalline morphology and monodisperse Ag NPs of sizes ranging from 23 to 41 nm. Furthermore, the metal-sensing activity of biosynthesized Ag NPs was evaluated using various metal ions; they were utilized for highly selective and sensitive colorimetric detection of Hg^{2+} in an aqueous medium among various metal ion solutions tested with the detection limit of 0.5 mM using the UV-Vis spectrophotometer. Similarly, they were also shown to be effective for the nanocatalytic activity for degradation of methylene blue dye up to 81%. These studies demonstrated Ag NPs as potential candidates for selective detection of mercury in water resources, a tool for sensing the heavy metals and degradation of synthetic dye from industrial effluents in wastewater treatment. Having the high surface-to-volume ratio and size-dependent functionality of Ag NPs, further optimization studies at micromolar and nanomolar detection limits will avail its better industrial utilization. Moreover, biologically mediated Ag NPs can also exhibit good antimicrobial activity against *Staphylococcus aureus* and *Escherichia coli*.

1. Introduction

Several nanomaterials have been produced by employing toxic chemicals for the manufacturing process and leaving hazardous waste materials behind, but most of them are dominated by metal-based nanomaterials: silver (Ag) and gold (Au). In recent years, silver nanoparticles (Ag NPs) have received significant attention in the chemical and physical approaches, aimed at reducing or eliminating the notorious materials for human health and the environment [1]. However, the manufacturing process somehow also poses a significant detrimental effect on the environment. In this

scenario, plant-mediated synthesis has been recognized as an alternative biological process for the production and functionalization of nanoparticles (NPs) [2]. Moreover, the biomolecules present in the plant extract consist of a large number of organic chemicals such as amides, carboxylic acids, polyphenols, flavonoids, terpenoids, and alkaloids, and some of these molecules are capable of donating electrons for the reduction of Ag^+ ions to Ag atoms [3]; also, they act as the capping and stabilizing agents leading to the formation of the Ag NPs [4]. Moreover, the biological techniques use the green chemistry principle to substitute potentially dangerous chemicals with natural products such as phytochemicals, enzymes, and biodegradable polymerase. Extracting diverse portions of plants (roots, leaf, and flower), microorganisms (extracellular and intracellular enzymes and metabolites), and biodegradable polymers might provide reducing agents for the synthesis, and these are superior to the physicochemical techniques of synthesis [4–7].

Several medicinal plants have already reported that they can be used to synthesize Ag NPs. Similarly, in this work, leaves of *R. arboreum*—a small tree or shrub with impressive red flowers—have been used as a phytoconstituent source. It is found in Asian countries, including China, Bhutan, Myanmar, Nepal, India, Sri Lanka, Pakistan, and Thailand. Furthermore, it is honored as a national flower of Nepal and has been used for various purposes for a long time. *R. arboreum* extracts and isolated compounds are found to have various biological activities such as antimicrobial, antioxidant, immunomodulatory, anti-inflammatory, hepatoprotective, adaptogenic, antidiarrheal, antidiabetic, and anticancer activities proving the plant's medicinal value which suggests it as a safe source of plant extract for the synthesis of Ag NPs [8]. Similarly, quercetin, a flavonol recovered from *R. arboreum*, has been demonstrated to have the largest zone of inhibition against microorganisms [9]. The flowers of *R. arboreum* have been used for medicinal purposes, while the plant's leaves have received less attention. Hence, the current study sought to investigate the range of biological activity of *R. arboreum* extracts.

During the synthesis of Ag NPs, physicochemical parameters such as pH, incubation temperature/duration, and concentration of silver nitrate and plant extracts play a crucial role in the particle size, shape, and stability of Ag NPs [9–12]. So, it is very critical to analyze these aspects for favorable research and industrial applications. The numerous applications of Ag NPs in different sectors have also extended to wastewater treatments [13] since the discharge of heavy metals and toxic chemicals in the environment, especially in the soil and water, raised a serious concern for the global ecosystem [10]. These metallic ions are considered systemic toxicants and classified as human carcinogens that are known to induce multiple organ damage [14], including the brain, kidney, nervous, and endocrine systems [15, 16]. In particular, there are several techniques available for the detection and quantification of heavy metals that need to be discussed. However, these techniques require expensive instrumentation and time-consuming sample preparation and preconcentration procedures [17]. Therefore, the colorimetric sensing technique is used for the detection of heavy metal ions in our research which has many advantages as compared to the other detection technique in terms of simplicity, rapidity, sensitivity, effectiveness, and ease of measurement [18, 19].

Similarly, organic dyes are widely regarded as the most hazardous pollutant having mutagenic and carcinogenic constituents while most the employee suffers from cancer, but no constituents are mentioned [20]; these remain in the environment for an extended period because of their greater stability which prevents them from being degraded easily. Consequently, many health-related issues have been identified, and several environmental risks associated with these toxic dyes are rife including kidney and liver damage, central nervous system poisoning, and skin problems as well as various blood disorders [21, 22]. Different physical and conventional methods are being used for dye degradation, such as activated carbon sorption, precipitation, flocculation, electrocoagulation, UV-light degradation, and redox treatments; ozonation is routinely used for dye degradation; however, these methods require high cost and energy and are associated with harmful side products and have limited success, leading to the need to develop an environmentally safe method [23–25]. Ag NPs are a possible alternative to traditional dye degradation processes because of their unique physicochemical and electronic properties, which are absent in bulk materials. Ag NPs are also well-known antimicrobial agents. It is generally accepted that Ag NPs interact with cell membranes, DNA, and microbial proteins of the microorganisms to produce antimicrobial effects [26]. Besides their metal-sensing, dye degradation, and antimicrobial applications, Ag NPs are also reported to exhibit antifungal, antiviral, anti-inflammatory, antiangiogenic, and anticancer activities along with diagnostic, biosensor, and gene therapy applications [27]. The goal of this study is to synthesize stable monodisperse Ag NPs from *R. arboreum* leaf extract with an optimal pH. They were characterized through UV-Vis, ATR-FTIR, XRD, SEM, EDX, and TEM. This is, to the best of our knowledge, the first assessment on the synthesis of Ag NPs using *R. arboreum*. Further, the metal ion-sensing capability, catalytic effect, and antibacterial activity of biosynthesized Ag NPs were investigated.

2. Material and Methods

2.1. Materials. *R. arboreum* leaves were collected from the Solukhumbu district of Nepal, with geographical distribution (27.3600°N, 86.6600°E). The plant was identified by the Tribhuvan University Central Herbarium. All the chemicals used in this work were of analytical grade. $AgNO_3$, ethanol, $CuCl_2{\cdot}2H_2O$, $ZnCl_2$, $HgCl_2$, $CdCl_2$, $CrCl_3{\cdot}6H_2O$, $Ni(NO_3)_2{\cdot}6H_2O$, and $FeCl_3$ were purchased from Sigma-Aldrich, USA. Furthermore, nutrient agar (NA) and Mueller Hinton agar (MHA) were purchased from HiMedia (India).

2.2. Preparation of Plant Extract. A sample of *R. arboreum* extract was prepared according to the method described in Gupta et al. [28] with some modifications. Briefly, 20 g of fresh leaves of *R. arboreum* was washed thoroughly with water, cut into fine pieces, and boiled in 100 mL distilled

water at 60°C for 30 min. The supernatant was collected using Whatman Filter Paper No. 1, and the freshly prepared extract was used in each set of experiments.

In the first set of experiments, a beaker containing a 1 : 9 ratio of *R. arboreum* aqueous extract and 1 mM $AgNO_3$ was agitated at 500 rpm for 15 min at 25°C. The pH of the reaction mixture was optimized to create monodispersed Ag NPs with adjustable size and shape.

The same approach was used in the second set of the experiment; however, the optimal pH of the reaction mixture was adjusted. The duration required for the complete reduction of silver ions to Ag NPs was determined by monitoring the *in situ* characterization of Ag NPs with a UV-Vis spectrophotometer at different time intervals of 10, 30, 60, 90, 120, and 150 min and 24 h to determine the time required for the complete reduction of silver ions to Ag NPs following a previously similar assayed method [29].

2.3. Separation of Ag NPs. After 24 h of incubation, the suspension was centrifuged at 9000 rpm for 20 min at 25° C, and the supernatant was then discarded; the pellet was redispersed in distilled water. To remove any adsorbed materials on the surface of Ag NPs, the centrifugation was repeated two times. The collected pellet was redispersed in absolute ethanol and then centrifuged. Purified Ag NPs were then dried at 30°C in an incubator and stored in an aluminum foil-wrapped Eppendorf tube for future analysis.

2.4. Characterization of Ag NPs. In situ characterization of Ag NPs was monitored using a UV-Vis spectrophotometer (SPECORD 200 Plus, Analytik Jena, scanning range 300-700 nm and resolution 1 nm). To determine the crystallinity of the Ag NPs powder, a routine powder X-ray diffraction pattern for dried Ag NPs was recorded using the Rigaku D/MAX-2500/pc diffractometer with monochromatic Cu Kα radiation of wavelength 1.54060 Å 2θ scanning between 20° and 80°. The crystallite size of powdered Ag NPs was determined via X-ray line broadening using Scherrer's equation [30].

The presence of secondary metabolites in the *R. arboreum* extract responsible for reducing Ag^+ to Ag NPs was investigated empirically using ATR-FTIR, with spectra scanned in the range of 4000–400 cm^{-1} (Nicolet iS50 FT-IR, Deuterated Tri-Glycine Sulfate (DTGS) detector). Scanning electron microscopy (SEM) data coupled with EDX (Jeol 6390LA/OXFORD XMX N) was used at an acceleration voltage of 20 kV. Nanoparticle size, grain size, size distribution, and morphology of synthesized Ag NPs were measured via HRTEM (Jeol/JEM 2100) at 200 kV with different magnification ranges.

2.5. Metal Ion-Sensing Activity of Ag NPs. Metal-sensing activity of Ag NPs was measured colorimetrically as described by Puente et al. [31]. In short, 1 mL of the metal solution was added to 4 mL (total 5 mL) of the Ag NP dispersion; the ions used for the tests were Cu(II), Ni(II), Hg(II) Cd(II), Zn(II), Fe(III), and Cr(III) at a concentration of 10 mM and were monitored using a UV-Vis spectrophotometer. Again, the concentration-dependent studies of Ag NPs with Hg^{2+} were carried out by adding different volumes (0-1000 μL) of 10 mM Hg(II) ion solution with 4 mL of Ag NPs, and then, water was added to maintain 5 mL. All resulting dispersion was diluted 9 folds, and the absorbance was measured.

2.6. Photocatalytic Activity of Ag NPs in Dye Degradation. The catalytic activity of Ag NPs was demonstrated by the degradation of methylene blue dye, as described by Jyoti and Singh [32]. In brief, as a stock solution, 10 mg of methylene blue was dissolved in 1 L of distilled water. Then, 1 mg of Ag NPs was added to 10 mL of methylene blue solution and mixed ultrasonically. After that, at a specific time interval, the 4 mL of each mixed solution was used to assess the catalytic degradation of methylene blue. The progress of the reaction was monitored using a UV-Vis spectrophotometer by measuring the absorbance maxima of the resulting solution at different time intervals, i.e., 1, 2, 3, 4, and 24 h. The percentage of dye degradation after 24 h was calculated using the following formula: %of decolorization = 100 $(A$? $- A)/A$?, where A? is the absorbance of the dye solution and A is the absorbance of the dye solution after catalytic degradation.

2.7. Antibacterial Activity of Ag NPs. The antibacterial activities of Ag NPs resulting from the *R. arboreum* extract were evaluated using the Kirby–Bauer Disc Diffusion Susceptibility Test [33]. The fresh culture of test organisms (*Escherichia coli* and *Staphylococcus aureus*) was spread on the MHA plate using a sterile cotton swab. Ag NPs (20 μL, 25 mg/500 μL), neomycin (1 mg/mL, positive control), and water (negative control) were all loaded separately onto the sterile blank antimicrobial susceptibility discs, which were later placed on the MHA plate and incubated at 37°C for 18-24 h. After proper incubation, the zone of inhibition (ZOI) was measured, and the results were recorded.

2.8. Data Analysis. All the acquired data were analyzed with the R-programming language (version 1.2.5033), and the ggplot2 (grammar of graphics 2, version 3.3.3) was used to create plots.

3. Results and Discussion

3.1. UV-Vis Spectroscopy Analysis. In particular, the UV-absorption measures the optical property in terms of surface plasmon resonance of Ag NPs which exhibits between 400 and 470 nm; that is affected by different extrinsic factors like pH, reaction time, and dielectric environment and intrinsic factors like shape, size, and morphology [34]. UV-Vis absorption data gives first-hand information at the very beginning of synthesis, which can be utilized to optimize the method of synthesis without going through extensive instrumental analysis [5]. Similarly, here in this study, with regard to the UV-Vis absorption spectrum, following the addition of the aqueous extract of *R. arboreum* to 1 mM $AgNO_3$, the color changed from yellow to dark brown since the reduction of the Ag^+ ions into Ag NPs has been harnessed to optimize the extrinsic factors like pH of the

medium and reaction time that affects the synthesis and stability of Ag NPs.

Moreover, the bandgap measurement is an essential metric in the study of nanomaterials. Insulators (>4 eV) or semiconductors (3 eV) can also be differentiated based on their bandgap energy [35], which is based on nanoparticle sizes; when the particle size of nanomaterials decreases, the bandgap energy increases [36]. The bandgap energy is determined to be in the range of 4.9 to 4.2eV using Planck's equation [37] which was coherent with our study, i.e., 4.7 eV based on our UV-Vis absorption peak (mentioned in very topic).

$$\text{Band gap energy } (E) = h \times \frac{C}{\lambda}, \tag{1}$$

where C is the speed of light = 3×10^8 m/s, h is Planck's constant = 6.626×10^{-34} J s, and λ is the cutoff wavelength = 400×10^{-9} to 470×10^{-9}.

3.2. Effect of pH on Ag NP Synthesis. The synthesis of Ag NPs via the aqueous extract of *R. arboreum* was performed over a pH range of 5.85–10, and Figure 1 shows the UV-Vis spectra of Ag NPs at various pH. In addition, these show the increasing pH of the reaction mixture, and the color of the solution changed from light yellow to yellowish brown to dark brown (Figure S1). The pH of a solution is an important parameter that affects the formation of Ag NPs because the pH can alter the charge of the biomolecules, which ultimately involves their capping and stabilizing abilities [38]. Experimental results demonstrated that almost no Ag NPs were produced at acidic pH at 25°C, whereas a strong SPR peak around 426 nm gradually occurred with an increase in pH of the reaction mixture from pH 5.85 to 9. A strong surface plasmon resonance (SPR) peak at 426 nm at pH 9 was observed and assigned the optimized pH. Upon further increasing the solution's pH 10, absorbance decreases due to the particles becoming unstable and agglomerated [39]. This indicates that the acidic pH, i.e., pH<7, suppressed the formation of Ag NPs, and pH 9 was the most favorable pH for the formation of Ag NPs using the leaf extract of *R. arboreum*. Furthermore, zeta potential shows significance in the study of nanomaterials and needs to be discussed. According to the literature, nanoparticles having zeta potentials greater than +30 mV or less than -30 mV are particularly stable in the dispersion medium [40]. These findings demonstrated that Ag NPs could maintain their structure over time and clearly show the effective production of Ag NPs.

3.3. Effect of Reaction Time on Ag NP Synthesis. The study for reducing the silver ions to Ag NPs was performed by considering the completion of the color change and monitoring the intensity of the UV-visible absorption peaks as a function of reaction time. Our results show the complete color change observed after 150 min (Figure S2). Similarly, Figure 2 shows no further increase in SPR intensity after 150 min. The SPR peak appeared only after 10 min of the addition of 10 mL of the extract of *R. arboreum* to 90 mL

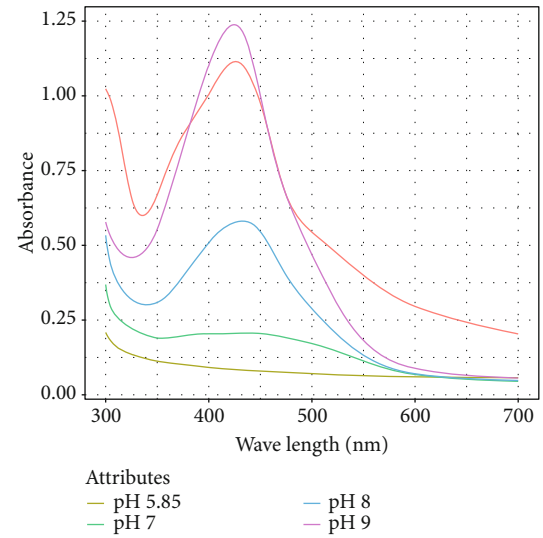

Figure 1: UV-Vis absorption spectra of green-synthesized silver nanoparticles at various pH values (pH 5.85, 7, 8, 9, and 10) of the reaction mixture.

of 1 mM $AgNO_3$ under pH 9 of the reaction mixture. Further, the intensity of the peak was increased as a function of time with no significant peak shift, indicating an enhancement in the formation of Ag NPs. It was found that the entire color change was observed after about 150 min; thereafter, there was no change in color of the reaction mixture, which was also confirmed by any incubation time beyond 150 min which showed almost no further increase in SPR intensity, suggesting that the silver salt present in the reaction mixture had been completely reduced within 150 min.

3.4. X-Ray Diffraction Analysis. The crystallinity property of *R. arboreum* extract-mediated synthesized Ag NPs is confirmed by the characteristic peaks observed in the XRD image (Figure 3). All of the diffraction peaks with indexed planes 38.16° (111), 44.24° (200), 64.60° (220), and 77.46° (311) are in good agreement with the face-centered cubic (fcc) silver lines of the powder data from JCPDS card number 04-0783 (Table S1). However, some other prominent peaks at 27.27°, 31.66°, and 45.74° could be due to the mixed phase of silver nanoparticles with the bioorganic phase (capping agent) or could be the formation of silver oxide in the incubation drying process [41, 42]. Here, the average crystallite or grain domain size was calculated using the Debye-Scherrer equation and was found to be 8.54 nm.

3.5. Attenuated Total Reflectance-Fourier Transform Infrared Spectroscopy Analysis. The leaves and twigs of *Rhododendron* are found to contain phenolic acids, which are described to have anti-HIV, anti-inflammatory, and antinociceptive activities [43]. Similarly, the possible role of phenolic acids in the reduction of Ag^+ ions to Ag NPs and stability in the form of a capping agent has been established through the ATR-FTIR study, where the Figure 4(a) spectrum shows

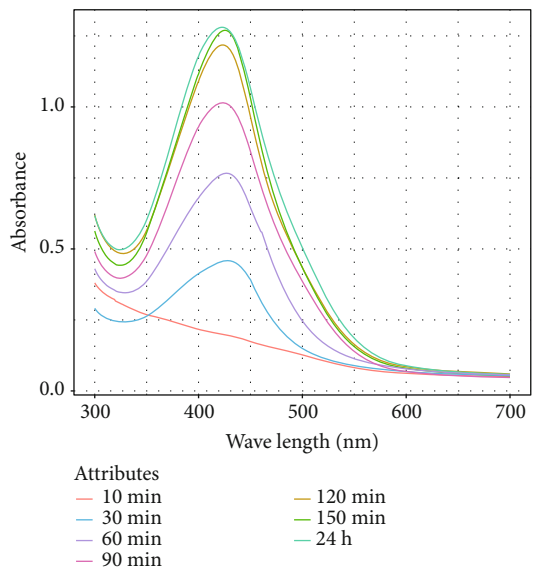

Figure 2: UV-Vis spectra were recorded at different time intervals, i.e., 10, 30, 60, 90, 120, and 150 min and 24 h of the addition of aqueous leaf extract of *R. arboreum* with aqueous silver nitrate solution under the optimum pH 9.

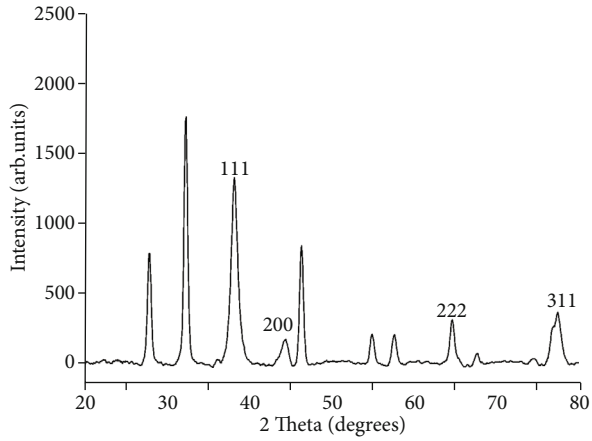

Figure 3: XRD pattern of Ag NPs showing the diffraction peaks synthesized using *R. arboreum* matching with the face-centered cubic of silver (fcc) JCPDS 04-0783.

the transmission peaks at 3307, 2383, 2350, 2324,1636, 1459, 1144, 1072, and 423 cm^{-1} for the leaf extract, whereas Figure 4(b) shows transmission peaks at 3726, 3583, 2920, 2383, 2350, 2324, 1610, 1550, 1511, 1052, 1033, 1013, and 666 cm^{-1} for Ag NPs synthesized from *R. arboreum*. Here, the spectrum appears to show the stretching of O-H and N-H; a broad and strong absorption band in the region of 3500-3000 cm^{-1} refers to the presence of phenolic acids which is shifted to the very weak band at ~3500 cm^{-1} and also proves the involvement of the phenolic functional group in the formation of Ag NPs, similarly like the role of citrate/ascorbate ions in the reducing, stabilizing, and complexing agent [44]. The absorption bands at 3726, 3583, and 3307 cm^{-1} refer to O-H stretching for the phenolic group in phenolic acids. The band 1634 cm^{-1} is caused by the C=C stretch of alkenes or the C=O stretch of amides. The change in wavelength from 1634 to 1544 cm^{-1} suggests that the (N-H)CO group has been linked to NPs. The peak at 1453 cm^{-1} is attributed to C-N stretching, probably due to the presence of an aliphatic amine group in the protein, as well as C-H bending, and it disappears in Ag NPs. C-stretching is responsible for the absorption at 1025-1200 cm^{-1}. The peak at 990 cm^{-1} might represent the =C-H group bending vibrations or C-H stretching of alkenes with side-chain vibrations, whereas the peak at 419 cm^{-1} could be ring-opening vibrations. The presence of =CH in aromatic compounds causes absorption at 650-850 cm^{-1}. The appearance of a 650 cm^{-1} peak might be attributed to carbohydrate ring deformation. All the above results make coherence with other similar work related to NPs based on green synthesis methods, which are also described by Dangi et al. [30].

3.6. Energy-Dispersive X-Ray Analysis. The EDX spectrum revealed the elementary composition of the biosynthesized Ag NPs (Figure 5) and demonstrated a definite signal of the metallic silver region at 3 keV, validating the synthesis of Ag NPs from the leaf extract of *R. arboreum*; further, the carbon and oxygen signals were also found. The result would correlate to the presence of Ag NPs capped with extract biomolecules owing to the presence of C and O, but it might also be from Ag_2O due to partial oxidation during drying as determined by XRD examination. According to the EDX results, the biosynthesized Ag NP contained 82.3% silver by weight (Figure 5, Table S2). Moreover, a similar study conducted by Femi-Adepoju et al. found 16% of silver by weight [45]; similarly, Dangi et al. have done a meticulous analysis of Ag NPs and found 27.63% of Ag NPs by weight [30]. Thus, our results suggest that this study has shown better results than the previous study with regard to the silver content on Ag NPs.

3.7. Transmission Electron Microscopy (TEM)/Scanning Electron Microscopy (SEM) Analysis. The size, shape, and morphology of Ag NPs were observed with TEM, where the micrographs revealed the spherical-shaped Ag NPs with an average diameter ranging between 23 and 41 nm (Figure 6). The TEM micrographs showed that the Ag NPs formed were predominantly monodisperse and uniform in size, proving that *R. arboreum* is an efficient source for the synthesis of Ag NPs. The crystallinity of Ag NPs was also analyzed through Selected Area Electron Diffraction (SAED), where the d-spacing calculated from the diffraction ring of SAED (8.021/nm) is in close agreement with the d-spacing obtained from the XRD and JCPDS 04-783 database shown in Table S3 [46]. Further, the scanning electron microscopy of Ag NPs produced from the *R. arboreum* confirms the formation of highly crystallite nanostructures that are roughly spherical (Figure S7). This image does not show significant results parallel to the TEM; thus, it is shown in the supplementary file.

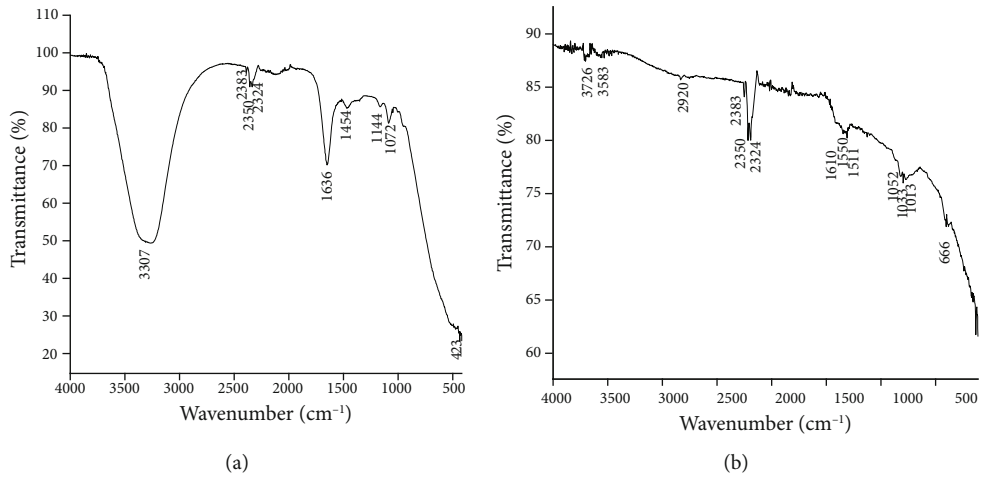

Figure 4: ATR-FTIR spectra of (a) aqueous plant extract and (b) Ag NPs synthesized using *R. arboreum*.

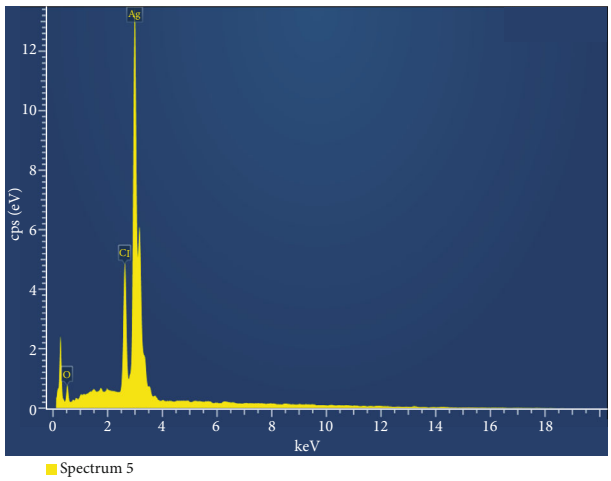

Figure 5: EDX spectrum of Ag NPs exhibiting the signal at 3 keV showing the presence of metallic silver.

3.8. Interaction of Ag NPs with Different Metal Ions and Detection of Hg^{2+}. The sensing characteristics of green-synthesized Ag NPs were tested for the colorimetric determination of Cu(II), Ni(II), Hg(II), Cd(II), Zn(II), Fe(III), and Cr(III) metal ions monitored using UV-visible spectroscopy (Figure 7). The Hg^{2+} metal ions changed the color of the Ag NP solution from dark brown to colorless, whereas the other metal ions had no significant effect on the color of the solution (Figure S3).

Hence, the prepared Ag NPs can detect Hg^{2+} ions in an aqueous medium using a colorimetric sensor. The color of the Ag NP solution was dark brown, and a characteristic SPR observed at 425 nm was the absence in the mixture of the resulting solution of Hg^{2+} ion and NPs. This could be due to Ag^0 being oxidized to Ag^+ during the reduction of Hg^{2+} ions [13]. The UV-visible spectra of the metal-sensing application of green-synthesized Ag NPs using *R. arboreum* obtained demonstrated that the addition of a known concentration of various metal ions has no obvious effect on the SPR band as compared to the Hg^{2+} ion shown in Figure 7. Thus, green-synthesized Ag NPs obtained using *R. arboreum* at pH 9 have very high selectivity and specificity towards Hg^{2+}. Similarly, Demir et al. used leaves of *Lantana camara* to synthesize Ag NPs for colorimetric sensing of Hg^{+2} [47]. The photographs taken after 10 min of adding different concentrations of Hg^{2+} to Ag NPs showed the visual color change of Ag NPs, which could be easily visualized by the naked eye as shown in Figure S4. Similarly, with an increase in the concentration of the Hg^{2+}, the intensity of SPR decreased gradually and shifted towards a lower wavelength along with the broadening of the SPR band, as shown in Figure S5. The influence of Hg^{2+} ions on the surface of Ag NPs with or without amalgamation, or a reduction in the size of the Ag NPs, could cause a decrease in the intensity of the SPR band with a blue shift [48]. As the concentration of the Hg^{2+} increases from 0.1 to 0.7 mM, the dispersion color gradually changes from dark brown to colorless. The minimum detectable concentration of the mercury ion was determined by the complete disappearance of the absorbance peak and was found to lie in the range of 0.5 to 0.6 mM.

3.9. Degradation of Methylene Blue: Catalytic Effects. The catalytic activity of Ag NPs on the degradation of methylene blue dye was monitored with a UV-Vis spectrophotometer. The absorption maxima for methylene blue dye in water were found to occur at 664 nm in the visible region [32]. The experimental result revealed a decrease in the color of the methylene blue solution with time which finally changed to colorless (Figure S6). The significant decline in the absorbance value of methylene blue dye approaching the baseline further verified the degradation of the dye (Figure 8). Finally, the peak of methylene blue disappeared with the increase in the reaction time. Photocatalysis is a key mechanism in dye effluent treatment, in which irradiated electrons are excited from the valence band to the conduction band, resulting in the formation of electron-hole pairs. The generated hydroxyl radical is a powerful oxidizing agent that completely degrades the dye

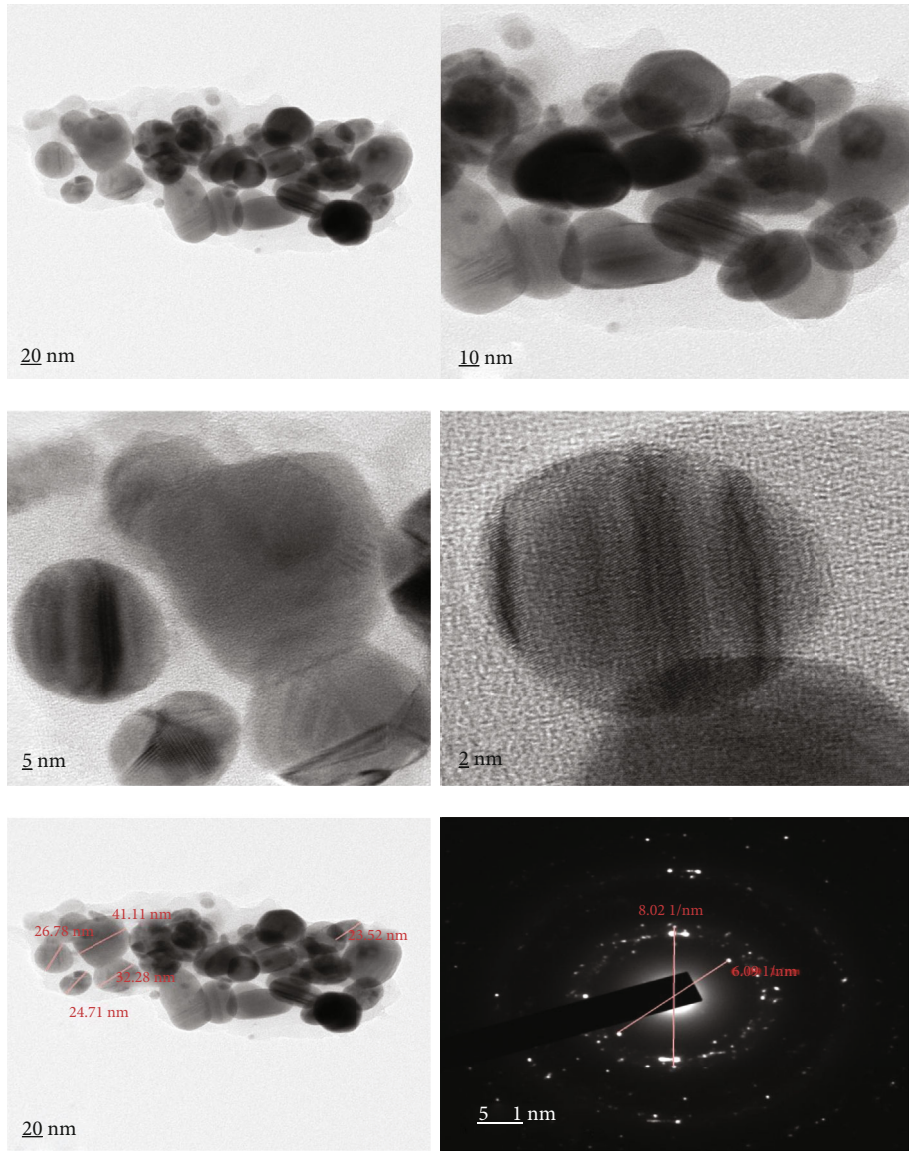

Figure 6: TEM and SAED images of Ag NPs at different scale bars (20, 10, 5, and 2 nm). The images show the monodisperse and spherical-shaped Ag NPs. The diameter obtained in the SAED data is used to measure the d-spacing (Table S3) which was compared with d-spacing with XRD data and JCPDS 04-0783.

into nonhazardous products (CO_2, H_2O, etc.) [49]. The percentage of degradation efficiency of silver nanoparticles was found as 81.87% at 24 h. The degradation percentage increased with increasing reaction time (Table 1). The methylene blue absorption peak was diminished and eventually disappeared as the reaction time was increased, indicating that the biosynthesized Ag NPs could degrade dye. Similarly, the green-synthesized Ag NPs from *Terminalia arjuna* leaves exhibited strong degradation of methylene blue (93.60%); completing the reduction reaction within 20 min was reported [50]. In our study, biosynthesized Ag NPs are less efficient degrading agents of methylene blue. The photodegradation of MB dye involves the generation of reactive species like hydroxy ($^{\cdot}OH$) radical and hole (h^+) by Ag NPs, which was evidenced by the active species trapping experiment performed by Kadam et al. [51]. Based on their experiment, the possible mechanism of generation of active species and degradation of MB can be outlined below.

$$\begin{aligned}
&Ag + h\nu \longrightarrow Ag^+\left[e^-(CB) + h^+(VB)\right]\\
&H_2O + h^+ \longrightarrow OH^{\cdot} + H^+\\
&O_2 + e^- \longrightarrow O_2^{-\cdot}\\
&O_2^{-\cdot} + H^+ \leftrightarrow HOO^{\cdot}\\
&2HOO^{\cdot} \longrightarrow H_2O_2 + O_2\\
&H_2O_2 \longrightarrow 2OH^{\cdot}\\
&MB + OH^{\cdot} \longrightarrow \text{degraded products}\\
&MB + h^+ \longrightarrow \text{oxidized products}\\
&MB + e^- \longrightarrow \text{reduced products}
\end{aligned} \tag{2}$$

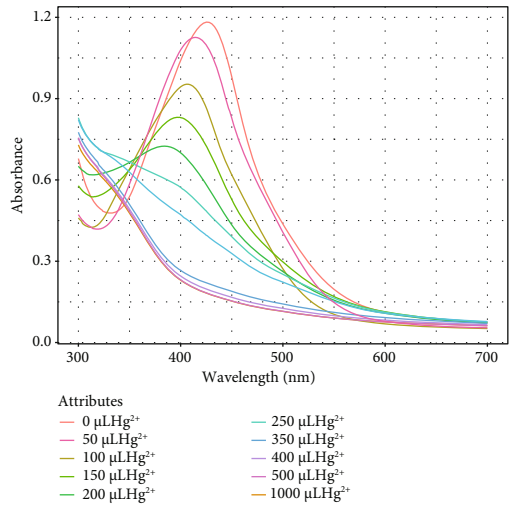

Figure 7: UV-Visible spectra recorded during metal-sensing application of different metals (Cu(II), Ni(II), Hg(II), Cd(II), Zn(II), Fe(III), and Cr(III)) using biosynthesized Ag NPs using *R. arboreum*.

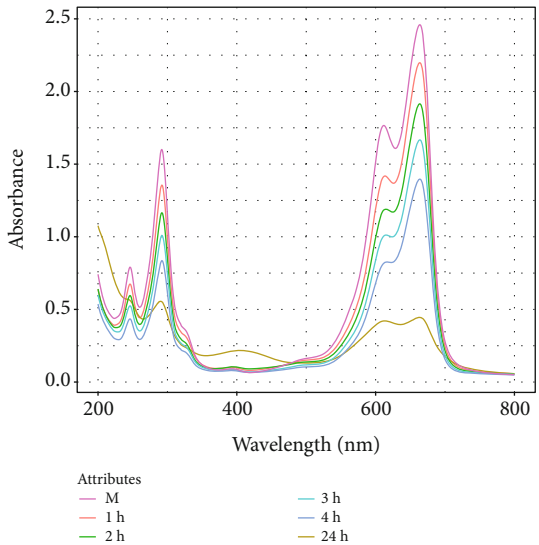

Figure 8: UV-Visible spectra illustrating the extent of methylene blue dye degradation in the presence of Ag NP catalyst at various time intervals (1, 2, 3, 4, and 24 h) in the visible region.

Table 1: Methylene blue degradation (%) by green-synthesized Ag NPs at different time intervals (1, 2, 3, 4, and 24 h).

Time (hours)	Amount of degradation (%)
1	10.64
2	22.15
3	32.24
4	43.23
24	81.87

Migration of electrons from Ag NPs plays a vital role in the degradation of dyes leading to nonhazardous products (CO_2, H_2O, etc.) [49, 52, 53].

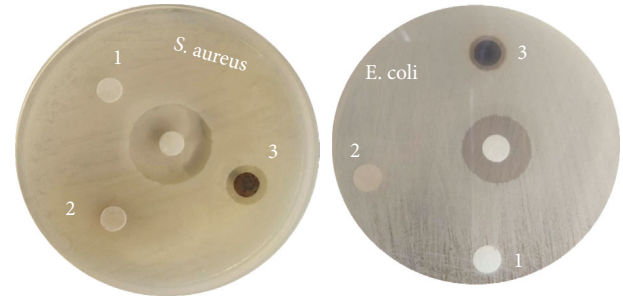

Figure 9: Antibacterial activity of Ag NPs against *S. aureus* and *E. coli* synthesized from *R. arboreum*. The activity was measured (Table S4) in terms of zone of inhibition (ZOI) with the standard antibiotic neomycin (center), distilled water (1), plant extract (2), and Ag NPs (3) using the disc diffusion method.

3.10. Antibacterial Activity of Ag NPs. The antibacterial activity of Ag NPs was studied using the diffuse disc method against both Gram-positive (*S. aureus*) and Gram-negative bacteria (*E. coli*). The biosynthesized Ag NPs showed better antibacterial activity against both types of bacteria (Figure 9). When compared to *E. coli*, Ag NPs had higher antibacterial activity against *S. aureus*, resulting in a larger zone of inhibition (Table S3). The antimicrobial activity of Ag NPs mostly depends on the structure of bacterial species, the final inoculated concentration of bacteria, pH, shape, size, and concentration of Ag NPs [54]. In addition, the biological activity of inorganic nanoparticles may be influenced by antibacterial activity: size distribution, shape, surface charge, surface chemistry, capping agents, and other variables are among them [51–53, 55, 56]. Moreover, the antibacterial activity of Ag NPs is due to the generation of reactive oxygen species (ROS) in the cellular environment that leads the DNA damage and disruptions of cellular activities. The possible detailed mechanisms of antibacterial activity have been discussed already by our groups in a previous article [5]. Accordingly, NPs may release silver ions, which enhance antibacterial properties by disabling respiratory chains, disrupting cell membranes, rupturing cellular contents, or attaching to functional groups of proteins, causing protein denaturation or blocking DNA replication [31, 54, 55, 57, 58]. In turn, Dangi et al. observed that green-synthesized Ag NPs showed the highest inhibition which was found on *K. pneumoniae* (12 mm) followed by *E. coli* (11 mm) and *S. aureus* (11 mm) with the least for *S. typhimurium* (7 mm) using the agar well diffusion method [30]. The release of silver ions was linked to the microbial activity of Ag NPs measuring 20–80 nm by several authors, whereas 10 nm Ag NPs proved more detrimental to *E. coli* due to the smaller size of the NPs [59]. In addition, the Ag NPs synthesized using *Murraya koenigii* (L.) (MK) revealed that the growth of all tested *S. aureus* strains was inhibited (~90%) in the presence of 32 μg/mL of MK-Ag NPs with ZOI 16 mm. Further, the sensitive strain of *E. coli* (21 mm) showed the least resistance to MK-Ag NPs with >81% inhibition at 16 μg/mL [60]. The inhibition potential of the freshly prepared *Oscillatoria limnetica* Ag NPs (22 mm against *E. coli* and 20 mm against *B. cereus*) was more relatively

pronounced than that induced by the tested antibiotics (19 mm for cefaxone and 18 mm for tetracycline) as reported by Hamouda et al. [61]. As a result, the antibacterial activity demonstrated by our sample could be due to the presence of bioactive molecules on the surface of silver nanoparticles which needs to be explored further for future applications.

4. Conclusions

In conclusion, the synthesis of biomediated Ag NPs using *R. arboreum* leaf extract critically depends on the pH and time of the reaction mixture. UV-visible spectroscopy results inferred that the formation of Ag NPs is in an aqueous medium, and X-ray diffraction (XRD) reveals the nature of Ag NPs, crystallite, and face center cubic structure of silver nanocrystals. ATR-FTIR spectroscopy confirmed the fabrication of Ag NPs using phytoconstituents, correspondingly like the reducing and stabilizing agents in chemical synthesis. Similarly, SEM and TEM analyses confirmed the formation of spherical-shaped Ag NPs with sizes ranging from 23.52 nm to 41.11 nm. The synthesized Ag NPs showed remarkably high sensitivity towards the Hg^{2+} compared to other metal ions and detected the Hg^{2+} ions in 0.5 to 0.6 mM. At the concentration of 0.6 mM of Hg^{2+} ions, the SPR of Ag NPs disappeared entirely, indicating the naked eye sensing limit. The synthesized Ag NPs are also used as a catalyst in the degradation of hazardous dyes; thus, they can be referred to as eco-friendly and cost-effective ways to use for sustainable goals in the environment. The efficiency of degradation is increased by increasing the time intervals. Hence, biosynthesized Ag NPs can be used in the purification of water and the treatment of effluent. Similarly, Ag NPs demonstrate good antibacterial activity against *E. coli* and *S. aureus in vitro*, paving the path for their possible topical administration against infections caused by those bacteria after careful *in vivo* testing. As a result, we believe that *R. arboreum* leaves could be a viable option in nanotechnology. Further research into pharmacological aspects *R. arboreum* should be carried out to help with future concerns.

Abbreviations

NPs: Nanoparticles
UV-vis: Ultraviolet-visible
XRD: X-ray diffraction
ATR-FTIR: Attenuated total reflectance-Fourier transform infrared
SEM: Scanning electron microscopy
TEM: Transmission electron microscopy
SPR: Surface plasmon resonance
MHA: Mueller Hinton agar
ZOI: Zone of inhibition
SAED: Selected area electron diffraction.

Data Availability

The data used to support the findings of this study are included within the article.

Conflicts of Interest

The authors declare that there is no conflict of interest regarding the publication of this paper.

Authors' Contributions

Niranjan Parajuli designed the research project. Sitaram Phuyal investigated the nanoparticles. Ganesh Lamichhane and Aaksh Gupta analyzed the data. Sitaram Phuyal and Karan Khadayat performed antimicrobial assays. Ganesh Lamichhane, Anup Adhikari, Aakash Gupta, and Niranjan Parajuli wrote the manuscript. Sujan Khadka and Rishab Marahatha revised the manuscript. All authors approved this manuscript.

Acknowledgments

The authors gratefully acknowledge the Sophisticated Test and Instrumentation Centre, Cochin University of Science and Technology campus, Kochi 682 022, Kerala, India.

Supplementary Materials

Figure S1: different colors of the reaction mixture at various pH values taken after 24 h of addition. Figure S2: color change of plant extract after addition of $AgNO_3$ as a function of reaction time. Figure S3: the interaction of freshly prepared silver nanoparticles with different metal ions. Figure S4: the interaction of freshly prepared silver nanoparticles with various concentrations of Hg^{2+} ions. Figure S5: the concentration-dependent UV-visible absorption studies of green-synthesized Ag NPs from *R. arboreum* with Hg^{2+} ion. Figure S6: change in color of the methylene blue solution after 24 h of the addition of Ag NPs. Figure S7: SEM images of Ag NPs at different scale bars. Table S1: crystallite size determination of Ag NPs from XRD. Table S2: the biosynthesized Ag NPs' elementary composition. Table S3: d-spacing calculation from SAED and comparison with XRD and JCPDS database. Table S4: antibacterial activity of green-synthesized Ag NPs. *(Supplementary Materials)*

References

[1] J. L. Hernández-Pinero, M. Terrón-Rebolledo, R. Foroughbakhch et al., "Effect of heating rate and plant species on the size and uniformity of silver nanoparticles synthesized using aromatic plant extracts," *Applied Nanoscience*, vol. 6, no. 8, pp. 1183–1190, 2016.

[2] M. Shah, D. Fawcett, S. Sharma, S. K. Tripathy, and G. E. J. Poinern, "Green synthesis of metallic nanoparticles via biological entities," *Materials*, vol. 8, no. 11, pp. 7278–7308, 2015.

[3] H. Barabadi, "Nanobiotechnology: a promising scope of gold biotechnology," *Cellular and Molecular Biology*, vol. 63, no. 12, pp. 3-4, 2017.

[4] S. Rajeshkumar and L. V. Bharath, "Mechanism of plant-mediated synthesis of silver nanoparticles - a review on biomolecules involved, characterisation and antibacterial activity," *Chemico-Biological Interactions*, vol. 273, pp. 219–227, 2017.

[5] S. Dawadi, S. Katuwal, A. Gupta et al., "Current research on silver nanoparticles: synthesis, characterization, and applications," *Journal of Nanomaterials*, vol. 2021, Article ID 6687290, 23 pages, 2021.

[6] H. Barabadi, F. Mojab, H. Vahidi et al., "Green synthesis, characterization, antibacterial and biofilm inhibitory activity of silver nanoparticles compared to commercial silver nanoparticles," *Inorganic Chemistry Communications*, vol. 129, p. 108647, 2021.

[7] M. Saravanan, H. Barabadi, H. Vahidi et al., "Chapter 19-Emerging theranostic silver and gold nanobiomaterials for breast cancer: present status and future prospects," in *Handbook on Nanobiomaterials for Therapeutics and Diagnostic Applications*, K. Anand, M. Saravanan, B. Chandrasekaran, S. Kanchi, S. J. Panchu, and Q. Chen, Eds., pp. 439–456, Elsevier, 2021.

[8] P. Rawat, N. Rai, N. Kumar, and R. K. Bachheti, "Review on Rhododendron arboreum - a magical tree," *Oriental Pharmacy and Experimental Medicine*, vol. 17, no. 4, pp. 297–308, 2017.

[9] P. K. Sonar, R. Singh, and S. K. Saraf, *Phytochemical and Biological Screening of Rhododendron arboreum (Sm.): Phytochemistry and Biology on R. arboreum*, LAP LAMBERT Academic Publishing, 2012.

[10] A. J. Kora, R. B. Sashidhar, and J. Arunachalam, "Gum kondagogu (Cochlospermum gossypium): a template for the green synthesis and stabilization of silver nanoparticles with antibacterial application," *Carbohydrate Polymers*, vol. 82, no. 3, pp. 670–679, 2010.

[11] A. K. Mittal, Y. Chisti, and U. C. Banerjee, "Synthesis of metallic nanoparticles using plant extracts," *Biotechnology Advances*, vol. 31, no. 2, pp. 346–356, 2013.

[12] Z.-R. Mashwani, T. Khan, M. A. Khan, and A. Nadhman, "Synthesis in plants and plant extracts of silver nanoparticles with potent antimicrobial properties: current status and future prospects," *Applied Microbiology and Biotechnology*, vol. 99, no. 23, pp. 9923–9934, 2015.

[13] K. Farhadi, M. Forough, R. Molaei, S. Hajizadeh, and A. Rafipour, "Highly selective Hg^{2+} colorimetric sensor using green synthesized and unmodified silver nanoparticles," *Sensors and Actuators B: Chemical*, vol. 161, no. 1, pp. 880–885, 2012.

[14] P. B. Tchounwou, C. G. Yedjou, A. K. Patlolla, and D. J. Sutton, "Heavy metal toxicity and the environment," in *Molecular, Clinical and Environmental Toxicology: Volume 3: Environmental Toxicology*, A. Luch, Ed., pp. 133–164, Springer, Basel, 2012.

[15] T. W. Clarkson, L. Magos, and G. J. Myers, "The toxicology of mercury — current exposures and clinical manifestations," *The New England Journal of Medicine*, vol. 349, no. 18, pp. 1731–1737, 2003.

[16] Y. Wang, F. Yang, and X. Yang, "Colorimetric biosensing of mercury(II) ion using unmodified gold nanoparticle probes and thrombin-binding aptamer," *Biosensors & Bioelectronics*, vol. 25, no. 8, pp. 1994–1998, 2010.

[17] A. Fan, Y. Ling, C. Lau, and J. Lu, "Direct colorimetric visualization of mercury (Hg^{2+}) based on the formation of gold nanoparticles," *Talanta*, vol. 82, no. 2, pp. 687–692, 2010.

[18] S. K. Ghosh and T. Pal, "Interparticle coupling effect on the surface plasmon resonance of gold nanoparticles: from theory to applications," *Chemical Reviews*, vol. 107, no. 11, pp. 4797–4862, 2007.

[19] C. Han, L. Zhang, and H. Li, "Highly selective and sensitive colorimetric probes for Yb3+ ions based on supramolecular aggregates assembled from beta-cyclodextrin-4,4'-dipyridine inclusion complex modified silver nanoparticles," *Chemical Communications*, vol. 24, no. 24, pp. 3545–3547, 2009.

[20] V. K. Vidhu and D. Philip, "Catalytic degradation of organic dyes using biosynthesized silver nanoparticles," *Micron*, vol. 56, pp. 54–62, 2014.

[21] O. Lefebvre and R. Moletta, "Treatment of organic pollution in industrial saline wastewater: a literature review," *Water Research*, vol. 40, no. 20, pp. 3671–3682, 2006.

[22] I. Mohmood, C. B. Lopes, I. Lopes, I. Ahmad, A. C. Duarte, and E. Pereira, "Nanoscale materials and their use in water contaminants removal—a review," *Environmental Science and Pollution Research*, vol. 20, no. 3, pp. 1239–1260, 2013.

[23] R. Patel and S. Suresh, "Decolourization of azo dyes using magnesium-palladium system," *Journal of Hazardous Materials*, vol. 137, no. 3, pp. 1729–1741, 2006.

[24] L. Gomathi Devi, S. Girish Kumar, K. Mohan Reddy, and C. Munikrishnappa, "Photo degradation of methyl orange an azo dye by advanced Fenton process using zero valent metallic iron: influence of various reaction parameters and its degradation mechanism," *Journal of Hazardous Materials*, vol. 164, no. 2-3, pp. 459–467, 2009.

[25] P. Kumar, M. Govindaraju, S. Senthamilselvi, and K. Premkumar, "Photocatalytic degradation of methyl orange dye using silver (Ag) nanoparticles synthesized from Ulva lactuca," *Colloids and Surfaces. B, Biointerfaces*, vol. 103, pp. 658–661, 2013.

[26] J. Yun and D. G. Lee, "Chapter 6-silver nanoparticles: a novel antimicrobial agent," in *Antimicrobial Nanoarchitectonics*, A. M. Grumezescu, Ed., pp. 139–166, Elsevier, 2017.

[27] X.-F. Zhang, Z.-G. Liu, W. Shen, and S. Gurunathan, "Silver nanoparticles: synthesis, characterization, properties, applications, and therapeutic approaches," *International Journal of Molecular Sciences*, vol. 17, no. 9, p. 1534, 2016.

[28] A. Gupta, A. R. Koirala, B. Joshi, S. Khanal, B. Gupta, and N. Parajuli, "Synthesis of silver nanoparticles using leaves of taraxacum officinale and their antimicrobial activities," *Advanced Science, Engineering and Medicine*, vol. 9, no. 3, pp. 221–228, 2017.

[29] M. M. H. Khalil, E. H. Ismail, K. Z. El-Baghdady, and D. Mohamed, "Green synthesis of silver nanoparticles using olive leaf extract and its antibacterial activity," *Arabian Journal of Chemistry*, vol. 7, no. 6, pp. 1131–1139, 2014.

[30] S. Dangi, A. Gupta, D. K. Gupta, S. Singh, and N. Parajuli, "Green synthesis of silver nanoparticles using aqueous root extract of _Berberis asiatica_ and evaluation of their antibacterial activity," *Chemical Data Collections*, vol. 28, p. 100411, 2020.

[31] C. Puente, I. Gómez, B. Kharisov, and I. López, "Selective colorimetric sensing of Zn(II) ions using green-synthesized silver nanoparticles: Ficus benjamina extract as reducing and stabilizing agent," *Materials Research Bulletin*, vol. 112, pp. 1–8, 2019.

[32] K. Jyoti and A. Singh, "Green synthesis of nanostructured silver particles and their catalytic application in dye degradation," *Journal, Genetic Engineering & Biotechnology*, vol. 14, no. 2, pp. 311–317, 2016.

[33] Y. Y. Loo, Y. Rukayadi, M. A. R. Nor-Khaizura et al., "In vitro antimicrobial activity of green synthesized silver nanoparticles

against selected Gram-negative foodborne pathogens," *Frontiers in Microbiology*, vol. 9, 2018.

[34] K. L. Kelly, E. Coronado, L. L. Zhao, and G. C. Schatz, "The optical properties of metal nanoparticles: the influence of size, shape, and dielectric environment," *The Journal of Physical Chemistry. B*, vol. 107, no. 3, pp. 668–677, 2003.

[35] D. Sundeep, T. Vijaya Kumar, P. S. S. Rao, R. V. S. S. N. Ravikumar, and A. Gopala Krishna, "Green synthesis and characterization of Ag nanoparticles from Mangifera indica leaves for dental restoration and antibacterial applications," *Progress in Biomaterials*, vol. 6, no. 1-2, pp. 57–66, 2017.

[36] M. Singh, M. Goyal, and K. Devlal, "Size and shape effects on the band gap of semiconductor compound nanomaterials," *Journal of Taibah University for Science*, vol. 12, no. 4, pp. 470–475, 2018.

[37] R. Ma, V. Sharma, A. F. Baldwin et al., "Rational design and synthesis of polythioureas as capacitor dielectrics," *Journal of Materials Chemistry A*, vol. 3, no. 28, pp. 14845–14852, 2015.

[38] M. Sathishkumar, K. Sneha, and Y.-S. Yun, "Immobilization of silver nanoparticles synthesized using Curcuma longa tuber powder and extract on cotton cloth for bactericidal activity," *Bioresource Technology*, vol. 101, no. 20, pp. 7958–7965, 2010.

[39] C. K. Tagad, S. R. Dugasani, R. Aiyer, S. Park, A. Kulkarni, and S. Sabharwal, "Green synthesis of silver nanoparticles and their application for the development of optical fiber based hydrogen peroxide sensor," *Sensors and Actuators B: Chemical*, vol. 183, pp. 144–149, 2013.

[40] K. C. dos Santos, M. F. G. da Silva, E. R. Pereira-Filho, J. B. Fernandes, I. Polikarpov, and M. R. Forim, "Polymeric nanoparticles loaded with the 3,5,3′-triiodothyroacetic acid (Triac), a thyroid hormone: factorial design, characterization, and release kinetics," *Nanotechnology, Science and Applications*, vol. 5, pp. 37–48, 2012.

[41] S. Gupta, P. Rautela, C. Maharana, and K. P. Singh, "Priming host defense against biotic stress by arbuscular mycorrhizal fungi," in *Agro-Environmental Sustainability: Volume 1: Managing Crop Health*, J. S. Singh and G. Seneviratne, Eds., pp. 255–270, Springer International Publishing, Cham, 2017.

[42] N. Khandan Nasab, Z. Sabouri, S. Ghazal, and M. Darroudi, "Green-based synthesis of mixed-phase silver nanoparticles as an effective photocatalyst and investigation of their antibacterial properties," *Journal of Molecular Structure*, vol. 1203, p. 127411, 2020.

[43] V. Kumar, S. Suri, R. Prasad et al., "Bioactive compounds, health benefits and utilization of Rhododendron: a comprehensive review," *Agriculture & Food Security*, vol. 8, no. 1, 2019.

[44] X. C. Jiang, C. Y. Chen, W. M. Chen, and A. B. Yu, "Role of citric acid in the formation of silver nanoplates through a synergistic reduction approach," *Langmuir*, vol. 26, no. 6, pp. 4400–4408, 2010.

[45] A. G. Femi-Adepoju, A. O. Dada, K. O. Otun, A. O. Adepoju, and O. P. Fatoba, "Green synthesis of silver nanoparticles using terrestrial fern (*Gleichenia Pectinata* (Willd.) C. Presl.): characterization and antimicrobial studies," *Heliyon*, vol. 5, no. 4, p. e01543, 2019.

[46] A. Gupta, A. R. Koirala, B. Gupta, and N. Parajuli, "Improved method for separation of silver nanoparticles synthesized using the Nyctanthes arbor-tristis shrub," *Acta Chemica Malaysia*, vol. 3, no. 1, pp. 35–42, 2019.

[47] D. Demir, N. Bölgen, and A. Vaseashta, *Green synthesis of silver nanoparticles using Lantana camara leaf extract and their use as mercury(II) ion sensor*, Advanced Nanotechnologies for Detection and Defence against CBRN Agents, Dordrecht, 2018.

[48] T. Morris, H. Copeland, E. McLinden, S. Wilson, and G. Szulczewski, "The effects of mercury adsorption on the optical response of size-selected gold and silver nanoparticles," *Langmuir*, vol. 18, no. 20, pp. 7261–7264, 2002.

[49] S. Marimuthu, A. J. Antonisamy, S. Malayandi et al., "Silver nanoparticles in dye effluent treatment: a review on synthesis, treatment methods, mechanisms, photocatalytic degradation, toxic effects and mitigation of toxicity," *Journal of Photochemistry and Photobiology. B*, vol. 205, p. 111823, 2020.

[50] S. Raj, H. Singh, R. Trivedi, and V. Soni, "Biogenic synthesis of AgNPs employing _Terminalia arjuna_ leaf extract and its efficacy towards catalytic degradation of organic dyes," *Scientific Reports*, vol. 10, no. 1, p. 9616, 2020.

[51] J. Kadam, P. Dhawal, S. Barve, and S. Kakodkar, "Green synthesis of silver nanoparticles using cauliflower waste and their multifaceted applications in photocatalytic degradation of methylene blue dye and Hg^{2+} biosensing," *SN Applied Sciences*, vol. 2, no. 4, 2020.

[52] W. Qing, K. Chen, Y. Wang, X. Liu, and M. Lu, "Green synthesis of silver nanoparticles by waste tea extract and degradation of organic dye in the absence and presence of H_2O_2," *Applied Surface Science*, vol. 423, pp. 1019–1024, 2017.

[53] V. Srivastava, S. Pandey, A. Mishra, and A. K. Choubey, "Green synthesis of biogenic silver particles, process parameter optimization and application as photocatalyst in dye degradation," *SN Applied Sciences*, vol. 1, no. 12, 2019.

[54] M. P. Patil and G.-D. Kim, "Eco-friendly approach for nanoparticles synthesis and mechanism behind antibacterial activity of silver and anticancer activity of gold nanoparticles," *Applied Microbiology and Biotechnology*, vol. 101, no. 1, pp. 79–92, 2017.

[55] H. Barabadi, A. Mohammadzadeh, H. Vahidi et al., "Penicillium chrysogenum-derived silver nanoparticles: exploration of their antibacterial and biofilm inhibitory activity against the standard and pathogenic Acinetobacter baumannii compared to tetracycline," *Journal of Cluster Science*, pp. 1–14, 2021.

[56] N. Talank, H. Morad, H. Barabadi et al., "Bioengineering of green-synthesized silver nanoparticles: in vitro physicochemical, antibacterial, biofilm inhibitory, anticoagulant, and antioxidant performance," *Talanta*, vol. 243, p. 123374, 2022.

[57] R. A. Bapat, T. V. Chaubal, C. P. Joshi et al., "An overview of application of silver nanoparticles for biomaterials in dentistry," *Materials Science and Engineering: C*, vol. 91, pp. 881–898, 2018.

[58] S. Ahmed, M. Ahmad, B. L. Swami, and S. Ikram, "A review on plants extract mediated synthesis of silver nanoparticles for antimicrobial applications: a green expertise," *Journal of Advanced Research*, vol. 7, no. 1, pp. 17–28, 2016.

[59] R. Salomoni, P. Léo, A. F. Montemor, B. G. Rinaldi, and M. F. A. Rodrigues, "Antibacterial effect of silver nanoparticles in Pseudomonas aeruginosa," *Nanotechnology, Science and Applications*, vol. 10, pp. 115–121, 2017.

[60] F. A. Qais, A. Shafiq, H. M. Khan et al., "Antibacterial effect of silver nanoparticles synthesized using Murraya koenigii (L.) against multidrug-resistant pathogens," *Bioinorganic Chemistry and Applications*, vol. 2019, Article ID e4649506, 11 pages, 2019.

[61] R. A. Hamouda, M. H. Hussein, R. A. Abo-elmagd, and S. S. Bawazir, "Synthesis and biological characterization of silver nanoparticles derived from the cyanobacterium _Oscillatoria limnetica_," *Scientific Reports*, vol. 9, no. 1, p. 13071, 2019.